Inorganic Chemistry

ARTICLE

pubs.acs.org/IC

Synthesis and Properties of Oxo-carboxylato- and Dioxo-Bridged Diosmium Complexes of Tris(2-pyridylmethyl)amine

Hideki Sugimoto,*[,†] Kazuhiro Kitayama,[†] Kenji Ashikari,[†] Chikako Matsunami,[‡] Naomi Ueda,[‡] Keisuke Umakoshi,[§] Yuko Hosokoshi,[⊥] Yoichi Sasaki,*[,‡,¶] and Shinobu Itoh*[,†]

[†]Department of Materials and Life Science, Division of Advanced Science and Biotechnology, Graduate School of Engineering, Osaka University, 2-1 Yamadaoka, Suita, Osaka 565-0871, Japan

[‡]Division of Chemistry, Graduate School of Science, Hokkaido University, Kita-ku, Sapporo 060-0810, Japan

[§]Division of Chemistry and Material Science, Graduate School of Engineering, Nagasaki University, Bunkyo-machi, Nagasaki 852-8521, Japan

[⊥]Department of Physical Science, Graduate School of Science, Osaka Prefecture University, Sakai, Osaka 599-8531, Japan

[¶]Catalysis Research Center, Hokkaido University, Kita-ku, Sapporo 001-0021, Japan

Supporting Information

ABSTRACT: A series of oxo-bridged diosmium complexes with tpa ligand (tpa = tris(2-pyridylmethyl)amine) are synthesized. The hydrolytic reaction of the mononuclear osmium complex $[Os^{III}Cl_2(tpa)]PF_6$ in aqueous solution containing a sodium carboxylate yields a μ-oxo-μ-carboxylato-diosmium(III) complex, $[Os^{III}_2(\mu\text{-}O)(\mu\text{-}RCOO)(tpa)_2](PF_6)_3$ (R = C_3H_7 (**1**), CH_3 (**2**), or C_6H_5 (**3**)). One-electron oxidation of **1** with $(NH_4)_2Ce^{IV}(NO_3)_6$ gives a mixed-valent $[Os^{III}Os^{IV}(\mu\text{-}O)(\mu\text{-}C_3H_7COO)(tpa)_2](PF_6)_4$ complex (**4**). A mixed-valent di-μ-oxo-diosmium complex, $[Os^{III}Os^{IV}(\mu\text{-}O)_2(tpa)_2](PF_6)_3$ (**5**), is also synthesized from **1** in an aerobic alkaline solution (pH 13.5). All the complexes exhibit strong absorption bands in a visible−near-infrared region based on interactions of the osmium dπ and oxygen pπ orbitals of the Os−O−Os moiety. The X-ray crystallographic analysis of **1**, **3**, and **4** shows that the osmium centers take a pseudo-octahedral geometry in the μ-oxo-μ-carboxylato-diosmium core. The mixed-valent osmium(III)osmium(IV) complex **4** has a shorter osmium−oxo bond and a larger osmium−oxo−osmium angle as compared with those of the diosmium(III) complex **1** having the same bridging carboxylate. Crystal structure of **5** reveals that the two osmium ions are bridged by two oxo groups to give an $Os_2(\mu\text{-}O)_2$ core with the significantly short osmium−osmium distance (2.51784(7) Å), which is indicative of a direct osmium−osmium bond formation with the bond order of 1.5 ($\sigma^2\pi^2\delta^2\delta^{*2}\pi^{*1}$ configuration). In the electrochemical studies, the μ-oxo-μ-carboxylato-diosmium(III) complexes exhibit two reversible $Os^{III}Os^{III}/Os^{III}Os^{IV}$ and $Os^{III}Os^{IV}/Os^{IV}Os^{IV}$ oxidation couples and one irreversible redox wave for the $Os^{III}Os^{III}/Os^{II}Os^{III}$ couple in CH_3CN. The irreversible reductive process becomes reversible in CH_3CN/H_2O (1:1 Britton−Robinson buffer; pH 5−11), where the $\{1H^+/2e^-\}$ transfer process is indicated by the plot of the redox potentials against the pH values of the solution of **1**. Thus, the μ-oxo-μ-butyrato-diosmium(III) center undergoes proton-coupled electron transfer to yield a μ-hydroxo-μ-butyrato-diosmisum(II) species. The di(μ-oxo) complex **5** exhibits one reversible $Os^{III}Os^{IV}/Os^{IV}Os^{IV}$ oxidation process and one reversible $Os^{III}Os^{IV}/Os^{III}Os^{III}$ reduction process in CH_3CN. The comproportionation constants K_{com} of the $Os^{III}Os^{IV}$ states for the present diosmium complexes are on the order of 10^{19}. The values are significantly larger when compared with those of similar oxo-bridged dimetal complexes of ruthenium and rhenium.

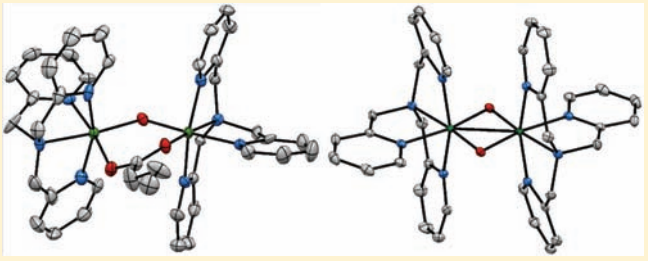

INTRODUCTION

Oxo-bridged dinuclear transition-metal complexes of the group 7 and 8 elements have long been attracting much attention due to their distinctive electronic and magnetic properties as well as chemical reactivities.[1−4] A large number of oxo-bridged-di-iron and -dimanganese complexes (3d-block elements) have been prepared as the model compounds of dinuclear metal active sites of various metalloproteins.[5,6] On the other hand, oxo-bridged dinuclear complexes of the 4d- and 5d-block elements of group 7 and 8 are featured with much stronger dπ(metal)−pπ-(bridging oxo) interactions and stronger metal−metal bonding interactions in a doubly bridged unit such as $M_2(\mu\text{-}O)_2$.[2,3] Such interactions bring various interesting aspects to these dinuclear metal centers, such as electronic communications and redox properties.[2,3] In addition, the substitution-inert nature of these metal ions in the

Received: June 9, 2011
Published: August 09, 2011

Chart 1. Chemical Structures of Complexes 1−5

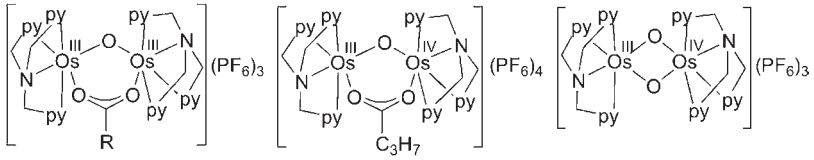

R = C_3H_7: **1**
= CH_3: **2**
= C_6H_5: **3**

4

5

oxidation states of +2, +3, and +4 enables us to isolate various types of oxo-bridged dinuclear metal complexes. These complexes could also be relevant to structural and functional models of dinuclear metalloproteins because isolation of di-iron and dimanganese model complexes in higher oxidation states is often difficult owing to their substitution-labile nature.

Although preparation methods for the oxo-bridged dinuclear metal complexes of Re (5d-block of the group 7 elements) and Ru (4d-block of the group 8 elements) have been well documented,[1−6] those for the oxo-bridged diosmium complexes have been limited to diosmium(IV), -(V), and -(VI) complexes. Namely, singly oxo-bridged $L_nOs^{III/IV}(\mu\text{-}O)Os^{IV}L_n$ (L = monodentate- or didentate-ligands),[7] doubly oxo-bridged $[Os^{VI}O_2X_2(\mu\text{-}O)_2Os^{VI}O_2X_2]^{4-}$ (X = CN^-, Cl^-, and OH^-, or X_2 = oxalate^{2-}),[8] and oxo-di-acetate bridged $Os^{IV}Cl_2PPh_3(\mu\text{-}O)(\mu\text{-}CH_3COO)_2Os^{IV}Cl_2PPh_3$ complexes have been synthesized.[9] Unfortunately, most of them contain simple monodentate external ligands. Thus, systematic investigations of oxo-bridged-diosmium complexes coordinated with common multidentate ligands have yet to be accomplished.

Recently, we prepared μ-oxo-μ-carboxylato-diruthenium(III)[10] and di-μ-oxo-rhenium(III)rhenium(IV) and -dirhenium(IV) complexes[11−13] with tris(2-pyridylmethyl)amine (tpa), which is one of the most popular tripodal tetradentate ligands. This stimulated us to target oxo-bridged diosmium complexes with tpa to compare their structures and electronic and redox properties with those of a series of the group 8 elements (iron and ruthenium) and with those of a group 7 element (rhenium) having the identical ligand. In this study, we have developed a series of oxo-bridged diosmium complexes with tpa. The synthesis and characterization of new oxo-bridged diosmium complexes with tpa, i.e., μ-oxo-μ-carboxylato-diosmium(III) (**1**−**3**) and its mixed-valent osmium(III)osmium(IV) derivative (**4**), as well as a mixed-valent di-μ-oxo-osmium(III)osmium(IV) complex (**5**), are described. The complexes **1**−**3** complete a set of isostructural μ-oxo-μ-carboxylato-dimetal(III) complexes of the group 8 elements.[10,14] On the other hand, the complex **5** is useful to compare the metal−metal interaction with that of the rhenium analogue (neighboring group element).[11] The complexes prepared in this study are given in Chart 1 together with their compound numbers.

EXPERIMENTAL SECTION

General Methods. All reagents and solvents were used as received unless otherwise noted. $[Os^{III}Cl_2(tpa)]PF_6$ was prepared according to the reported procedure.[15]

Preparation of the Complexes. *$[Os^{III}_2(\mu\text{-}O)(\mu\text{-}C_3H_7COO)(tpa)_2](PF_6)_3$* (***1***). To an aqueous solution (15 mL) of sodium butylate (2.37 g, 54 mmol) was added 150 mg (0.383 mmol) of $[Os^{III}Cl_2(tpa)]PF_6$, and the mixture was refluxed for 45 min to give a deep blue solution. Upon addition of NH_4PF_6 (70 mg, 0.43 mmol) at room temperature, a deep blue precipitate was formed. The solid was collected by filtration, washed with diethyl ether, and dried in vacuo. Yield 255 mg (0.170 mmol) 89%. IR (KBr): 1530 cm^{-1} (ν_{syn}(OCO)), 1450 (ν_{asyn}(OCO)). UV−vis (CH_3CN): λ_{max} = 245 nm (ε = 29 700 M^{-1} cm^{-1}), 368 (12 800), 398 (13 200), 500 (8370), 585 (14 700), 802 (2640), 1100 (1200), 1180 (1270), 1260 (1160). ^{1}H NMR (CD_3CN): δ = 1.43 ppm (s, 3 H), 1.74 (s, 2 H), 2.90−3.03 (m, 5 H), 3.43 (tt, 1 H, J_1 = 7.8, J_2 = 2.4 Hz), 4.18 (s, 2 H), 5.74 (d, 1 H, J = 7.8 Hz), 6.55−6.61 (m, 4 H), 6.72 (d, 2 H, J = 15.6 Hz), 6.83 (d, 1 H, J = 5.5 Hz), 7.24 (d, 2 H, J = 4.6 Hz), 7.32−7.42 (m, 7 H), 7.46 (td, 1 H, J_1 = 7.8 Hz, J_2 = 1.4 Hz), 7.55 (d, 1 H, J = 6.0 Hz), 7.59 (d, 2 H, J = 15.2 Hz), 8.37 (d, 2 H, J = 7.8 Hz), 9.59 (t, 2 H, J = 6.4 Hz), 9.79 (d, 1 H, J = 7.8 Hz), 10.04 (d, 2 H, J = 15.1 Hz), 10.75 (t, 1 H, J = 6.2 Hz), 11.81 (d, 2 H, J = 15.1 Hz). Anal. Calcd for **1** ($C_{40}H_{43}N_8O_3F_{18}P_3Os_2$): C, 32.05; H, 2.89; N, 7.47%. Found: C, 32.23; H, 2.78; N, 7.57%.

$[Os^{III}_2(\mu\text{-}O)(\mu\text{-}CH_3COO)(tpa)_2](PF_6)_3$ (***2***). This complex was prepared similar to **1** except using sodium acetate instead of sodium butylate. Yield 85%. The deep blue solid was recrystallized from acetone−water. IR (KBr): 1540 cm^{-1} (ν_{syn}(OCO)), 1450 (ν_{asyn}(OCO)). UV−vis (CH_3CN): λ_{max} = 313 nm (ε = 11 000 M^{-1} cm^{-1}), 373 (15 200), 420 (13 700), 760 (4430), 1194 (1120). ^{1}H NMR (CD_3CN): δ = 1.72 ppm (s, 2 H), 2.61 (s, 3 H), 4.13 (s, 2 H), 5.72 (d, 1 H, J = 7.8 Hz), 6.55−6.62 (m, 5 H), 6.72 (d, 2 H, J = 15.6 Hz), (d, 1 H, J = 6.0 Hz), 7.24 (d, 2 H, J = 5.0 Hz), 7.36 (tt, 7 H, J_1 = 13.5, J_2 = 5.5 Hz), 7.46 (td, 1 H, J_1 = 7.8, J_2 = 1.4 Hz), (t, 1 H, J = 6.4 Hz), 7.64 (d, 2 H, J = 15.1 Hz), 8.36 (d, 2 H, J = 6.9 Hz), 9.58 (t, 2 H, J = 6.6 Hz), 9.79 (d, 1 H, J = 7.8 Hz), 10.04 (d, 2 H, J = 15.1 Hz), 10.73 (t, 1 H, J = 6.4 Hz), 11.78 (d, 2 H, J = 15.1 Hz). Anal. Calcd for **2**·$2H_2O$ ($C_{38}H_{43}N_8O_5F_{18}P_3Os_2$): C, 30.28; H, 2.88; N, 7.43%. Found: C, 29.92; H, 2.60; N, 7.25%.

$[Os^{III}_2(\mu\text{-}O)(\mu\text{-}C_6H_5COO)(tpa)_2](PF_6)_3$ (***3***). This complex was prepared similar to **1** except using sodium benzoate instead of sodium butylate. Yield 83%. IR (KBr): 1520 cm^{-1} (ν_{syn}(OCO)), 1450 (ν_{asyn} (OCO)). UV−vis (CH_3CN): λ_{max} = 245 nm (ε = 20 900 M^{-1} cm^{-1}), 369 (9200), 400 (8900), 502 (4900), 582 (8130), 804 (1320), 1097 (920), 1169 (960), 1253 (957). ^{1}H NMR (CD_3CN): δ = 3.72 ppm (t, 1 H, J = 7.6 Hz), 4.23 (s, 2 H), 5.89 (d, 1 H, J = 7.8 Hz), 6.44 (d, 2 H, J = 15.2 Hz), 6.67 (t, 2 H, J = 8.6 Hz), 6.70 (d, 2 H, J = 6.8 Hz), 7.06 (d, 1 H, J = 5.5 Hz), 7.26−7.50 (m, 12 H), 7.61 (t, 1 H, J = 6.4 Hz), 7.94 (t, 2 H, J = 7.8 Hz), 8.24 (t, 1 H, J = 7.6 Hz), 8.35 (d, 2 H, J = 7.3 Hz), 9.44 (t, 2 H, J = 6.4 Hz), 9.67 (d, 2 H, J = 15.2 Hz), 9.68 (d, 1 H, J = 6.4 Hz), 9.95 (d, 2 H, J = 8.0 Hz), 10.70 (t, 1 H, J = 6.4 Hz), 11.45 (d, 2 H, J = 15.1 Hz). Anal. Calcd for **3** ($C_{43}H_{41}N_8O_3F_{18}P_3Os_2$): C, 33.69; H, 2.70; N, 7.31%. Found: C, 33.94; H, 2.62; N, 7.08%.

$[Os^{III}Os^{IV}(\mu\text{-}O)(\mu\text{-}C_3H_7COO)(tpa)_2](PF_6)_4$ (***4***). To a deep blue solution of **1** (150 mg, 0.100 mmol) in acetone−water (6 mL, 1:1 v/v) was added cerium(IV)ammonium nitrate (CAN) (56 mg, 0.102 mmol), whereupon the color of the solution changed to dark brown. The solution was stirred for 1 h. Upon addition of NH_4PF_6 (65 mg, 0.399 mmol) at room temperature, a dark brown precipitate was formed. The solid was collected by

dx.doi.org/10.1021/ic201230k |*Inorg. Chem.* 2011, 50, 9014–9023

Table 1. Crystallographic Data for 1, 3·2CH$_3$CN, 4·(CH$_3$)$_2$CO, and 5·2CH$_3$CN

	1	3·2CH$_3$CN	4·(CH$_3$)$_2$CO	5·2CH$_3$CN
formula	$C_{40}H_{43}F_{18}N_8Os_2P_3O_3$	$C_{47}H_{47}F_{18}N_{10}O_3Os_2P_3$	$C_{43}H_{49}F_{24}N_8O_4Os_2P_4$	$C_{40}H_{42}F_{18}N_{10}O_2Os_2P_3$
formula weight	1499.12	1615.25	1702.17	1510.13
crystal system	monoclinic	monoclinic	monoclinic	monoclinic
space group	$P2_1/n$ (No. 14)	$P2_1/c$ (No. 14)	$P2_1/c$ (No. 14)	$C2/c$ (No. 15)
a, Å	14.4134(15)	12.0808(12)	19.587(7)	21.7247(6)
b, Å	18.326(2)	19.3190(18)	12.304(5)	11.6280(3)
c, Å	18.2725(19)	23.521(2)	23.333(8)	20.8290(5)
β, deg	90.5371(17)	100.4270(10)	91.838(4)	113.0153(8)
V, Å^3	4826.3(9)	5398.9(9)	5620(3)	4842.9(2)
Z	4	4	4	4
D_{calcd}, g cm^{-3}	2.063	1.987	2.012	2.071
T, K	113	113	113	108
μ(Mo Kα), cm^{-1}	54.748	49.033	47.576	54.566
$2\theta_{max}$, deg	55.0	55.0	55.0	55.0
no. of reflns ($I > 2\sigma I_0$)	7801	10587	8408	5522
no. of reflns (all data)	10753	12192	12703	5171
no. of variables	710	749	767	361
$R1^a$ ($I > 2\sigma I_0$)	0.0342	0.0365	0.0648	0.0179
$wR2^b$ (all data)	0.0545	0.1568	0.1611	0.0454
GOF	0.904	0.656	0.786	1.045

$^a R1 = \Sigma||F_o| - |F_c||/\Sigma|F_o|$. $^b wR2 = [\Sigma(w(F_o^2 - F_c^2)^2)/\Sigma w(F_o^2)^2]^{1/2}$.

filtration, washed with diethyl ether, and dried in vacuo. The dark brown solid was recrystallized from acetone−water. Yield 137 mg (83%). IR (KBr): 1510 cm^{-1} (ν_{syn}(OCO)), 1440 (ν_{asyn}(OCO)). UV−vis (CH$_3$CN: λ_{max} = 245 nm (ε = 38 400 M^{-1} cm^{-1}), 375 (16 200), 405 sh (15 000), 504 (7970), 583 (14 500), 807 (1830), 1094 (760). Anal. Calcd for **4**·acetone·H$_2$O ($C_{43}H_{51}N_8O_5F_{24}P_4Os_2$): C, 30.02; H, 2.99; N, 6.51%. Found: C, 29.74; H, 2.67; N, 6.47%.

[Os^{III}Os^{IV}(μ-O)$_2$(tpa)$_2$](PF$_6$)$_3$ (***5***). Solid of **2** (366.5 mg, 0.25 mmol) was added to an aqueous solution (30 mL, pH ca. 13.5) containing NaOH (400 mg, 10.0 mmol). The solution was stirred for 4 h at 80 °C, whereupon the color of the solution changed from deep violet to orange. After the solution was cooled to room temperature, an orange solid precipitated from the solution. The solid was collected by filtration and washed with a small volume of cold methanol to remove the remaining **2**. An additional washing with diethylether gave an orange powder. The orange powder was recrystallized from the acetonitrile solution. Yield 96.2 mg (0.064 mmol, 26%). IR (KBr): 890 cm^{-1} (OsO_2), 846, 560 (PF_6^-). UV−vis (CH$_3$CN: λ_{max} = 250 nm (ε = 25 700 M^{-1} cm^{-1}), 313 (10 780), 373 (15 440), 420 (13 870), 760 (4350), 1197 (1240). FAB−MS: m/z = 1284 ({[Os$_2$(μ-O)$_2$(tpa)$_2$](PF$_6$)$_2$}$^+$). Anal. Calcd for **5**·2CH$_3$CN ($C_{40}H_{42}N_{10}O_2F_{18}P_3Os_2$): C, 31.81; H, 2.80; N, 9.27%. Found: C, 31.41; H, 2.73; N, 9.23%.

Physical Measurements. FT−IR spectra were recorded with a Jasco FT−IR 4100 spectrometer. ^{1}H NMR spectra were recorded with a JEOL-ECP 400 or a JEOL-ECS 400, and the TMS signal was adjusted to 0 ppm. FAB−MS spectra were measured with a JEOL JMS−700S. UV−vis spectra were recorded on a Jasco V570 spectrometer. Static magnetic measurements were made using a Quantum Design MPMS superconducting quantum interference device (SQUID) magnetometer in the temperature range of 2−300 K and in magnetic fields up to 5 T. The diamagnetic contribution was subtracted from the overall magnetization signal by using Pascal's law.

Electrochemistry. Cyclic voltammetric measurements were performed under dinitrogen with a Hokuto Denko HZ−3000 potentiostat. A set of a glassy carbon working electrodes (circular, 3 mm diameter), a Ag/AgCl reference electrode, and a platinum counter electrode was employed in these experiments.

Scheme 1. Synthetic Scheme of Complexes 1−5

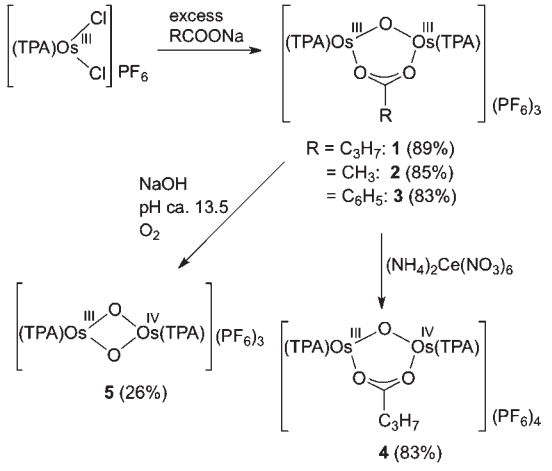

X-ray Crystallography. Single crystals of **1** and **3**·2CH$_3$CN were obtained by diffusion of diethylether into acetonitrile solutions of **1** and **3**. Single crystals of **4**·(CH$_3$)$_2$CO were obtained by slow evaporation of the acetone−water solution. Single crystals of **5**·2CH$_3$CN were grown by diffusion of diethylether into an acetonitrile solution of **5**. Each single crystal obtained was mounted on a loop with mineral oil, and all X-ray data except **5**·2CH$_3$CN were collected at −160 °C on a Rigaku CCD diffractometer with monochromatic Mo Kα radiation. The X-ray data of **5**·2CH$_3$CN were collected at −165 °C on a Rigaku R-AXIS RAPID diffractometer using filtered Mo Kα radiation. The structures were solved by direct methods (SIR 2008[16]) and expanded using Fourier techniques. The non-hydrogen atoms were refined anisotropically by full-matrix least-squares on F^2. The hydrogen atoms were attached at

dx.doi.org/10.1021/ic201230k |*Inorg. Chem.* 2011, 50, 9014–9023

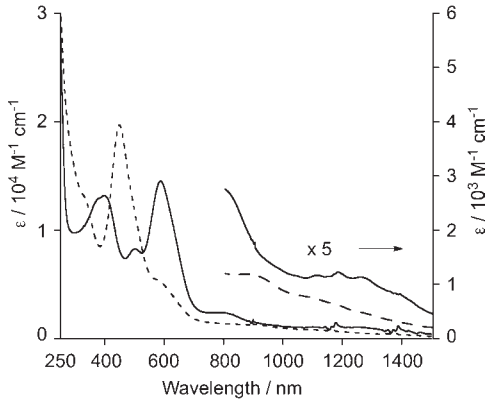

Figure 1. Absorption spectra of **1** (solid line) and **4** (dotted line) in CH_3CN.

idealized positions on carbon atoms and were not refined. All structures in the final stages of refinement showed no movement in the atom positions. The calculations were performed using Single-Crystal Structure Analysis Software, version 3.8.[17] Crystallographic parameters are summarized in Table 1.

RESULTS AND DISCUSSION

Synthesis and Characterization. We employed $[Os^{III}Cl_2(tpa)]PF_6$ as a starting compound and examined its hydrolytic reaction to obtain oxo-bridged diosmium(III) complexes. The synthetic routes are summarized in Scheme 1. When $[Os^{III}Cl_2(tpa)]PF_6$ was treated with 10 equiv of RCOONa (R = $CH_3C_2H_4$, CH_3, and C_6H_5) in H_2O (ca. pH 7.5) for 0.5 h under refluxing conditions, the starting material was recovered almost quantitatively. By increasing the amount of RCOONa from 10 to 140 equiv (pH 8.5−9.0) and the reaction time from 0.5 to 1 h, the μ-oxo-μ-carboxylato-diosmium(III) complexes (**1**−**3**) were obtained and isolated as their PF_6^- salts in high yield (83−89%) after addition of excess NH_4PF_6. Complexes **1**−**3** are the first oxo-bridged diosmium(III) compounds isolated. They complete a set of $M^{III}_2(\mu\text{-O})(\mu\text{-carboxylato})$ complexes (M = Os, Ru,[10] or Fe[14]) coordinated with the identical supporting ligand.

In the ^1H NMR spectra of **1**−**3**, sharp signals were observed in a range from 1.4 to 11.8 ppm (see Experimental Section), suggesting strongly antiferromagnetically coupled diosmium(III) centers in the complexes. The magnetic measurements of complexes **1** and **3** indicated that each osmium(III) center employs an $S = 1/2$. The magnetic behavior of these complexes can be explained by the zero field splitting (D) of the triplet ground state with $D = 2640-2850$ cm^{-1}. The μ-oxo-μ-carboxylato-diosmium(III) complexes exhibited strong absorption bands with molar extinction coefficients $>10^3$ M^{-1} cm^{-1} in a visible-to-near-IR region. The absorption spectrum of **1** is shown in Figure 1 (solid line) as a typical example, and those of the acetate and benzoate derivatives are given in Figures S1 and S2, respectively, in the Supporting Information. All the μ-oxo-μ-carboxylato-diosmium(III) complexes showed similar absorption spectra. The bands in the visible-to-near-IR region can be assigned to electronic transitions between molecular orbitals formed through interactions of the Os dπ and oxygen pπ orbitals of the Os−O−Os moiety because the oxo-bridged diruthenium(III) complexes such as $[Ru^{III}_2(\mu\text{-O})(\mu\text{-RCOO})_2(N,N',N''\text{-trimethyl-triazacyclononane})_2]^{2+}$ (R = CH_3, H_2Cl, Cl_3C, C_6H_5, H, CF_3), $[Ru^{III}_2(\mu\text{-O})(\mu\text{-}CH_3COO)_2(\text{pyridine})_6]^{2+}$, and $[Ru^{III}_2(\mu\text{-O})Cl_2(tpa)_2]^{2+}$ also show intense absorption bands based on transitions within the Ru−O−Ru core in a visible-to-near-IR region.[10,18] In particular, the absorption bands may be assigned on the basis of the Os−O−Os dπ−pπ−dπ molecular orbital scheme $(\pi_1^2\pi_2^2n_1^2n_2^2\pi^*_1{}^2\pi^*_2{}^0$ configuration for Os(III)−O−Os(III)). The bands in a visible region of **1** may be assigned to $\pi-\pi^*$ electronic transitions, while those in a near-IR region may be associated with weak electronic transitions from occupied π^* orbital to unoccupied π^* orbital.

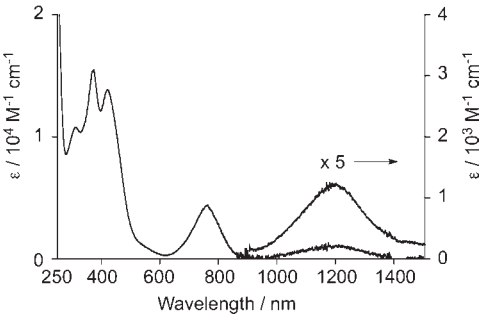

Figure 2. Absorption spectrum of **5** in CH_3CN.

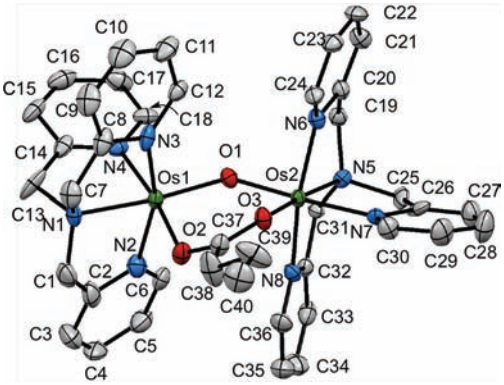

Figure 3. Crystal structure of the cationic part of **1** shown in 50% ellipsoids. The hydrogen atoms and solvent molecules were omitted for clarity.

The one-electron oxidized mixed-valent complex, **4**, was successfully isolated from the butyrate bridging complex, **1**, by oxidation with a cerium(IV) ion. Complex **4** is also the first example of mixed-valent μ-oxo-μ-carboxylato-osmium(III)osmium(IV) complex. The one-electron oxidation resulted in blue shift of the strong absorption bands of **1** in the visible-to-near-IR region (398 → 375, 585 → 504, 802 nm → 583 nm) because of the stabilized Os−O−Os dπ−pπ−dπ molecular orbital with $\pi_1^2\pi_2^2n_1^2n_2^2\pi^*_1{}^1\pi^*_2{}^0$ configuration in energy (Figure 1 (dotted line)).

The di-μ-oxo-diosmium complex could not be prepared directly from $[OsCl_2(tpa)]PF_6$ in an alkaline solution at pH 11−12 under refluxing conditions. The precursor was recovered in this case. However, the mixed-valent di-μ-oxo-osmium(III)osmium(IV) complex (**5**) was obtained in a 26% yield when the hydrolytic reaction of **2** was conducted in an alkaline solution at pH 13.5 under air under refluxing conditions. The complex **5** is the first di-μ-oxo-osmium(III)osmium(IV) complex. The absorption spectrum of **5** in acetonitrile is shown in Figure 2. The strong bands were observed at 313 nm (ε = 10 780 M^{-1} cm^{-1}),

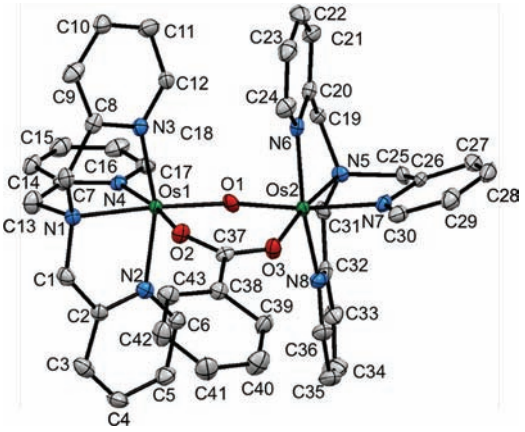

Figure 4. Crystal structure of the cationic part of $3\cdot 2CH_3CN$ shown in 50% ellipsoids. The hydrogen atoms and the solvent molecules were omitted for clarity.

371 (15 440), 420 (13 870), and 760 (4350) in the visible region. These bands may be assigned based on the molecular orbital scheme of Os−Os bonds ($\sigma^2\pi^2\delta^2\delta^{*2}\pi^{*1}\sigma^*$ configuration) and are ascribed to the $\pi-\pi^*$ transitions within the direct Os−Os bond in the $Os^{III}Os^{IV}(\mu\text{-}O)_2$ unit (see Crystal Structures). The band centered at 1197 nm (ε = 1240 M^{-1} cm^{-1}) may be assignable to transitions involving the half-filled π^* orbital.

Crystal Structures. *Complexes **1** and **3**.* The crystal structures of the cationic parts of **1** and **3** are shown in Figures 3 and 4, respectively. The selected bond distances and angles are listed in Table 2. The complex cation of **1** comprises two osmium ions bridged by one oxo group and one butylate ligand. Additional coordination by the four nitrogen atoms of tpa to each osmium ion provides a distorted octahedral coordination geometry of the metal center. In this case, the two osmium ions are not equivalent. Namely, tertiary amine nitrogen N(1) atom of one tpa is situated trans to the bridging oxygen O(1) atom, while that of another tpa (N(5)) is located trans to the O(3) atom of the bridging butylate ligand, giving a longer Os(1)−N(1) bond (2.111(4) Å) and a shorter Os(2)−N(5) bond (2.051(4) Å). Such a nonequivalent geometric structure is also found in the tpa-di-iron(III) and -diruthenium(III) analogues.[13,18] The Os(1)−Os(2) distance of **1** is 3.4481(2) Å and the Os(1)−O(1)−Os(2) angle is 131.33(18)°. Complex **3** has a similar asymmetric dinuclear structure bridged by one oxo group and one benzoate ligand. The dihedral angle between the Os(1)−O(2)−C(37) and Os(2)−O(3)−C(37) planes in **3** is 23°, which is significantly smaller than that of 47° in **1**. This is compatible with the longer Os(1)−Os(2) distance of 3.5468(2) Å and larger Os(1)−O(1)−Os(2) angle of 135.67(17) in **3** as compared with those of **1**. The Os−Os distances of **1** and **3** are appreciably longer than those of the ruthenium and iron analogues (3.399(1) Å for $[Ru^{III}_2(\mu\text{-}O)(\mu\text{-}PrCOO)(tpa)_2]^{3+}$ and 3.243(1) Å for $[Fe^{III}_2(\mu\text{-}O)(\mu\text{-}CH_3COO)(tpa)_2]^{3+}$).[13,18] Among these series, the M(1)−O(1)−M(2) bond angle becomes larger in going from ruthenium (127.9(3)°), to iron (129.2(3)°),[13,18] to osmium (131.31(16) and 135.67(17)°), indicating that the bridging O(1) atoms in the diosmium complexes have a larger contribution to sp hybridization. These inspections of the dimensions around the metal centers of the isostructural series reveal that $d\pi-p\pi$ interactions are more significant in the osmium complex.

Table 2. Selected Bond Lengths (Å) and Angles (°) of 1 and $3\cdot 2CH_3CN$

	1	$3\cdot 2CH_3CN$
Os(1)−O(1)	1.921(4)	1.914(3)
Os(1)−O(2)	2.099(4)	2.094(3)
Os(1)−N(1)	2.111(4)	2.106(4)
Os(1)−N(2)	2.073(5)	2.070(3)
Os(1)−N(3)	2.045(5)	2.068(4)
Os(1)−N(4)	2.027(4)	2.037(3)
Os(2)−O(1)	1.907(4)	1.915(3)
Os(2)−O(3)	2.080(4)	2.083(3)
Os(2)−N(5)	2.051(4)	2.059(4)
Os(2)−N(6)	2.053(4)	2.058(4)
Os(2)−N(7)	2.085(4)	2.094(4)
Os(2)−N(8)	2.071(4)	2.044(4)
Os(1)−Os(2)	3.4481(2)	3.5468(2)
O(2)−C(37)	1.262(6)	1.261(5)
O(3)−C(27)	1.261(6)	1.251(6)
O(1)−Os(1)−O(2)	93.39(14)	91.77(13)
O(1)−Os(1)−N(1)	174.23(16)	176.00(14)
O(1)−Os(1)−N(2)	105.70(16)	94.99(15)
O(1)−Os(1)−N(3)	93.50(16)	103.40(15)
O(1)−Os(1)−N(4)	95.34(16)	97.41(15)
O(2)−Os(1)−N(1)	88.62(15)	88.31(14)
O(2)−Os(1)−N(2)	89.87(15)	87.39(13)
O(2)−Os(1)−N(3)	90.22(15)	92.14(13)
O(2)−Os(1)−N(4)	170.95(15)	170.77(16)
N(1)−Os(1)−N(2)	79.69(17)	81.01(16)
N(1)−Os(1)−N(3)	81.08(17)	80.59(16)
N(1)−Os(1)−N(4)	82.46(17)	82.46(16)
N(2)−Os(1)−N(3)	160.76(17)	161.61(17)
N(2)−Os(1)−N(4)	90.03(16)	90.92(13)
N(3)−Os(1)−N(4)	86.91(16)	86.60(13)
O(1)−Os(2)−N(3)	92.48(13)	93.92(14)
O(1)−Os(2)−N(5)	94.81(15)	91.56(14)
O(1)−Os(2)−N(6)	93.47(15)	90.39(14)
O(1)−Os(2)−N(7)	176.32(15)	171.89(15)
O(1)−Os(2)−N(8)	88.51(15)	90.57(14)
O(3)−Os(2)−N(5)	172.56(14)	173.52(14)
O(3)−Os(2)−N(6)	94.53(14)	99.39(15)
O(3)−Os(2)−N(7)	90.70(14)	92.92(15)
O(3)−Os(2)−N(8)	101.00(14)	94.94(15)
N(5)−Os(2)−N(6)	83.55(15)	84.02(16)
N(5)−Os(2)−N(7)	81.96(15)	81.90(15)
N(5)−Os(2)−N(8)	80.72(15)	81.53(16)
N(6)−Os(2)−N(7)	84.44(16)	84.19(15)
N(6)−Os(2)−N(8)	164.25(16)	165.53(17)
N(7)−Os(2)−N(8)	92. 69(16)	93.18(15)
Os(1)−O(1)−Os(2)	131.33(18)	135.67(17)
O(2)−C(37)−O(3)	125.5(5)	127.1(4)
a	47	23

[a] Dihedral angle between Os(1)−O(2)−C(37)/Os(2)−O(3)−C(37) planes.

*Complex **4**.* The crystal structure of the cationic part of the mixed-valent complex **4** is shown in Figure 5. The selected bond

dx.doi.org/10.1021/ic201230k |*Inorg. Chem.* 2011, 50, 9014–9023

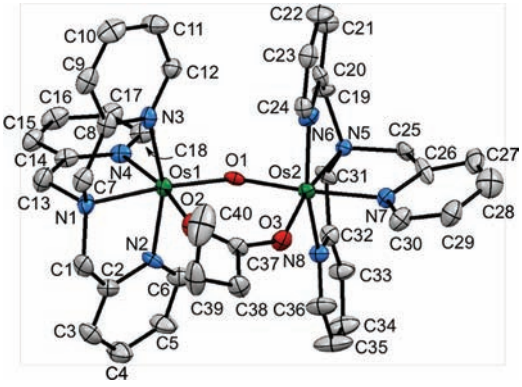

Figure 5. Crystal structure of the cationic part of **4**·$(CH_3)_2CO$ shown in 50% ellipsoids. The hydrogen atoms and the solvent molecule were omitted for clarity.

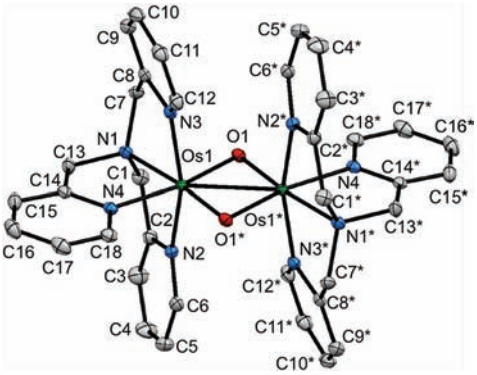

Figure 6. Crystal structure of the cationic part of **5**·$2CH_3CN$ shown in 50% ellipsoids. The hydrogen atoms and the solvent molecules were omitted for clarity.

Table 3. Selected Bond Lengths (Å) and Angles (°) of 4

Os(1)−O(1)	1.873(6)	Os(1)−O(2)	2.067(6)
Os(1)−N(1)	2.088(7)	Os(1)−N(2)	2.056(6)
Os(1)−N(3)	2.093(6)	Os(1)−N(4)	2.047(7)
Os(2)−O(1)	1.860(6)	Os(2)−O(3)	2.074(6)
Os(2)−N(5)	2.056(6)	Os(2)−N(6)	2.073(6)
Os(2)−N(7)	2.085(8)	Os(2)−N(8)	2.070(6)

O(1)−Os(1)−O(2)	90.1(3)	O(1)−Os(1)−N(1)	174.7(2)
O(1)−Os(1)−N(2)	94.4(3)	O(1)−Os(1)−N(3)	104.7(3)
O(1)−Os(1)−N(4)	101.2(3)	O(2)−Os(1)−N(1)	86.5(3)
O(2)−Os(1)−N(2)	90.8(3)	O(2)−Os(1)−N(3)	89.5(3)
O(2)−Os(1)−N(4)	168.5(3)	N(1)−Os(1)−N(2)	81.5(3)
N(1)−Os(1)−N(3)	79.4(3)	N(1)−Os(1)−N(4)	82.0(3)
N(2)−Os(1)−N(3)	160.9(3)	N(2)−Os(1)−N(4)	86.7(3)
N(3)−Os(1)−N(4)	89.3(3)	O(1)−Os(2)−N(3)	89.3(3)
O(1)−Os(2)−N(5)	99.7(3)	O(1)−Os(2)−N(6)	89.4(3)
O(1)−Os(2)−N(7)	172.6(3)	O(1)−Os(2)−N(8)	96.4(3)
O(3)−Os(2)−N(5)	170.6(3)	O(3)−Os(2)−N(6)	100.4(3)
O(3)−Os(2)−N(7)	88.8(3)	O(3)−Os(2)−N(8)	94.6(3)
N(5)−Os(2)−N(6)	82.6(3)	N(5)−Os(2)−N(7)	82.7(2)
N(5)−Os(2)−N(8)	81.7(3)	N(6)−Os(2)−N(7)	83. 9(2)
N(6)−Os(2)−N(8)	163.9 (3)	N(7)−Os(2)−N(8)	90.9(3)
Os(1)−O(1)−Os(2)	143.7(6)	O(2)−C(37)−O(3)	125.7(7)
Os(1)−O(2)−C(37) /Os(2)−O(3)−C(37)[a]	20		

[a] Dihedral angle.

Table 4. Selected Bond Lengths (Å) and Angles (°) of 5·2CH$_3$CN

Os(1)−O(1)	1.9822(13)	Os(1)−O(1)*	1.9676(13)
Os(1)−N(1)	2.0901(16)	Os(1)−N(2)	2.0069(3)
Os(1)−N(3)	2.065(2)	Os(1)−N(4)	2.0832(17)
Os(1)−Os(1)*	2.51784(7)		

O(1)−Os(1)−O(1)*	100.80(6)	Os(1)−O(1)−Os(1)*	79.20(5)
O(1)−Os(1)−N(1)	86.88(6)	O(1)−Os(1)−N(2)	91.24(7)
O(1)−Os(1)−N(3)	92.53(7)	O(1)−Os(1)−N(4)	167.54(6)
O(1)*−Os(1)−N(1)	172.31(6)	O(1)*−Os(1)−N(2)	99.30(7)
O(1)*−Os(1)−N(3)	97.08(7)	O(1)*−Os(1)−N(4)	91.62(6)

distances and angles are listed in Table 3. The tetracationic dinuclear core is isostructural with that of tricationic **1**, and their geometric configurations are very similar to each other. The Os(1)−O(1) and Os(1)−O(2) bond distances of 1.873(6) and 2.067(7) Å, respectively, are not significantly different from those of the Os(2)−O(1) and Os(2)−O(3) bonds (1.860(6) and 2.074(6) Å), suggesting that **4** is classified as class II in the Robin−Day's definition (somewhat spin-delocalized one). On the other hand, careful inspection of the dimensions around the Os(1) and Os(2) centers in **1** and **4** reveals some notable differences. First, both Os(1)−O(1) and Os(2)−O(1) bonds become shorter (1.921(3) and 1.907(4) Å → 1.873(6) and 1.860(6) Å) by one-electron oxidation of **1** to give **4**, indicating increasing sp hybridization character of the O(1) atom of **4**. Second, the enhanced electrostatic repulsion between the two osmium ions in **4** makes the Os(1)−Os(2) distance longer as compared with that of **1** (3.4481(2) → 3.5435(4) Å). This causes the larger Os(1)−O(1)−Os(2) angle (131.33(18) → 143.7(6)°) and smaller dihedral angle of Os(1)−O(2)−C(37) and Os(2)−O(3)−C(37) planes (47 → 20°) as compared with those of **1**.

Complex ***5***. The crystal structural analysis revealed that complex **5** adopts an edge shared di-μ-oxo-diosmium structure (Figure 6). The selected bond distances and angles are summarized in Table 4. Other coordination sites of each osmium center are occupied by four nitrogen atoms from tpa, giving the metal centers with a distorted octahedral stereochemistry. The diosmium center formally adopts an osmium(III)osmium(IV) mixed-valent state because the compound consists of one complex cation and three PF_6^- anions. The complex cation has a centrosymmetric configuration to give the crystallographically equivalent osmium centers. The Os(1)−Os(1)* distance of **5** is found to be 2.51784(7) Å, which is considerably shorter than those of the μ-oxo-μ-carboxylato-osmium(III)osmium(IV) complex **4** (3.5435(4) Å) and even shorter than the sum of the radii of two osmium atoms (2.70 Å),[19] indicating the existence of a direct metal−metal bonding interaction. This short Os(1)−Os(1)* bond makes the Os_2O_2 core have an acute Os(1)−O(1)−Os(1)* angle (79.20(5)°) and obtuse O(1)−Os(1)−O(1)* angles (100.80(6)°). Because the total number of 5d-electrons for the osmium(III)osmium(IV) state is nine, the electronic configuration

dx.doi.org/10.1021/ic201230k |*Inorg. Chem.* 2011, 50, 9014–9023

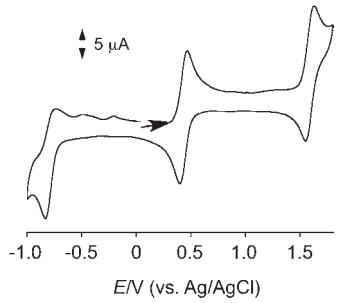

Figure 7. Cyclic voltammogram of **1** in acetonitrile containing $^{n}Bu_4NPF_6$ (0.1 M) with a scan rate of 100 mV/s.

of $\sigma^2\pi^2\delta^2\delta^{*2}\pi^{*1}$ with the bond order of 1.5 is expected for the osmium(III)osmium(IV) bond.

The Os−Os distance of **5** is longer than the Re−Re distance (2.426(1) Å) of the isostructural di-μ-oxo-rhenium(III)rhenium(IV) complex, $[Re^{III}Re^{IV}(\mu\text{-}O)_2(Metpa)_2](PF_6)_3$.[11] This is consistent with the expected higher bond order of 2.5 ($\sigma^2\pi^2\delta^2\delta^{*1}$) for the rhenium(III)rhenium(IV) complex. The even shorter Re−Re distances of the similar complexes, $[Re^{IV}_2(\mu\text{-}O)_2(tpa)_2](PF_6)_4$ (2.364(1) Å), $[Re^{IV}_2(\mu\text{-}O)_2(Metpa)_2]^{4+}$ (2.368(1) Å), and $[Re^{IV}_2(\mu\text{-}O)_2(Me_2tpa)_2]^{3+}$ (2.383(1) Å), are consistent with the expected Re−Re bond order of 3 with the electronic configuration of $\sigma^2\pi^2\delta^2$.[11,12] Thus, the metal−metal distances of the di-μ-oxo-dimetal complexes with tpa and its related ligands nicely follow the expected metal−metal bond order (in the parentheses) as follows: Os^{III}−Os^{IV} (1.5) > Re^{III}−Re^{IV} (2.5) > Re^{IV}−Re^{IV} (3).

Electrochemical Properties. *Complexes **1**−**4**.* The μ-oxo-μ-carboxylato-diosmium(III) complexes exhibited two oxidation processes and one reduction process in acetonitrile under a dinitrogen atmosphere. The cyclic voltammogram (CV) of **1** is shown in Figure 7 and those of **2** and **3** are given in Figures S3 and S4 (Supporting Information), respectively. The redox potentials are summarized in Table 5. The first and second oxidation processes were reversible within the time scale of the CV measurements. The two consecutive oxidation processes are assigned to $Os^{III}Os^{III}/Os^{III}Os^{VI}$ and $Os^{III}Os^{IV}/Os^{IV}Os^{IV}$ redox couples, respectively (Scheme 2a). The CV of **4** that is a one-electron oxidized complex of **1** was identical to that of **1** except for the different rest potential. The redox potentials ($E_{1/2}$ vs Ag/AgCl) for the oxidation processes move to more positive as the pK_a value of the corresponding carboxylic acid decreases, i.e., for PrCOOH (pK_a = 4.82): 0.42 and 1.58 V; for CH_3COOH (4.76): 0.45 and 1.60 V; and for C_6H_5COOH (4.21): 0.47 and 1.61 V. Namely, as the pK_a value of the carboxylic acid increases, the electron donation from the deprotonated carboxylate ligand to the diosmium center increases, which resulted in decreasing the redox potentials. The reduction processes of the three complexes were irreversible, which was tentatively assignable to an $Os^{III}Os^{III}/Os^{II}Os^{III}$ redox couple (Scheme 2a). The reduction potentials also move to more positive in the order of **1** < **2** < **3**.

The redox potentials for $Os^{III}Os^{III}/Os^{II}Os^{III}$ and $Os^{III}Os^{III}/Os^{III}Os^{IV}$ couples have more negative values as compared with those of the corresponding $Ru^{III}Ru^{III}/Ru^{II}Ru^{III}$ and $Ru^{III}Ru^{III}/Ru^{III}Ru^{IV}$ redox couples of the isostructural ruthenium analogue, $[Ru^{III}_2(\mu\text{-}O)(\mu\text{-}CH_3COO)(tpa)_2]^{3+}$, by ca. 0.45 V,[10] indicating stability of the higher oxidation states in the diosmium complexes as compared with the diruthenium analogues. A similar trend (ca. 0.55 V difference) was observed for a series of the isostructural mononuclear complexes $[MCl_2(tpa)]^+$ (M = Os^{III} and Ru^{III}).[15]

Table 5. Electrochemical Data of $[Os^{III}_2(\mu\text{-}O)(\mu\text{-}RCOO)(tpa)_2](PF_6)_3$ (1, 2, and 3) and $[Os^{III}Os^{IV}(\mu\text{-}O)_2(tpa)_2](PF_6)_3$ (5) Together with Those of the Ru (Ru^{III}_2OAc)[a] and Re ($Re^{III}Re^{IV}O_2$)[b] Analogues of 2 and 5

	$E_{1/2}$ $M^{II}M^{III}$/ $M^{III}M^{III}$ [c]	$E_{1/2}$ $M^{III}M^{III}$/ $M^{III}M^{IV}$ [c]	$E_{1/2}$ $M^{III}M^{IV}$/ $M^{IV}M^{IV}$ [c]	K_{com} [d]	ref
1	−0.73[e]	0.45	1.60	3.9×10^{19} [f]	
2	−0.75[e]	0.42	1.58	2.7×10^{19} [f]	
3	−0.70[e]	0.47	1.61	1.8×10^{19} [f]	
Ru^{III}_2OAc	−0.29	0.95			ref 18
5		−0.53	0.62	5.9×10^{19} [f]	
$Re^{III}Re^{IV}O_2$		−0.77	0.09	1.5×10^{13}	ref 15

[a] $[Ru^{III}_2(\mu\text{-}O)(CH_3COO)(tpa)_2](PF_6)_3$. [b] $[Re^{III}Re^{IV}(\mu\text{-}O)_2(tpa)_2](PF_6)_3$. [c] V vs Ag/AgCl in CH_3CN. [d] Equation 1. [e] Irreversible, E^{pa} value. [f] This work.

The $Ru^{III}Ru^{IV}/Ru^{IV}Ru^{IV}$ redox waves were not observed for the diruthenium complex as it is expected to appear in fairly positive potential >2.0 V. Stability of the $Os^{III}Os^{IV}$ mixed-valent state is indicated by the larger peak separation of the redox potentials for the $Os^{III}Os^{III}/Os^{III}Os^{IV}$ and $Os^{III}Os^{IV}/Os^{IV}Os^{IV}$ redox waves, which is represented by the comproportionation constant (K_{com}) defined by eq 1. The K_{com} values were calculated to be 2.7×10^{19}, 3.9×10^{19}, and 1.8×10^{19} for the butyrate, acetate, and benzoate complexes, respectively (Table 5).

$$K_{com} = [Os^{III}Os^{IV}]^2/[Os^{III}_2][Os^{IV}_2] = \exp(F\Delta E/RT) \quad (1)$$

The pH-dependent CVs of **1** were measured in CH_3CN/Britton−Robinson buffer (1:1) solvent system under a dinitrogen atmosphere in order to study the influence of protonation at the oxide bridge on the redox potentials. The pH range examined was pH 5−10.5 because the redox wave of the $Os^{III}Os^{III}/Os^{II}Os^{III}$ process became irreversible below pH 5. The CV of **1** at pH 8.0 is shown in Figure 8a, where the current area to the reductive process is almost double to that of the oxidative process. The redox potential of the oxidation process ($Os^{III}Os^{III}/Os^{III}Os^{IV}$) appears to be pH-independent, indicating that protonation at the bridging oxo group does not occur during the oxidation process of $Os^{III}Os^{III}/Os^{III}Os^{IV}$ in the pH range studied. On the other hand, the reduction wave moved to the negative direction as the solution pH increased as shown in Figure 8b. A plot of the redox potential against the solution pH from 5 to 10.5 is shown in Figure 8c. The reduction potential shows linear dependence on pH with the slope of 0.029 V per pH unit, indicating that the corresponding redox process involves one-proton plus two-electron transfer ($1H^+/2e^-$). Hence, the process can be assigned to an $Os^{III}(\mu\text{-}O)Os^{III}/Os^{II}(\mu\text{-}OH)Os^{II}$ couple, where protonation occurs at the bridging oxo group upon two-electron reduction (Scheme 2b). Such a $1H^+/2e^-$ process may be observed when the following conditions are fulfilled: (i) the reduction to the $Os^{II}(\mu\text{-}O)Os^{III}$ state causes the simultaneous protonation at the bridging oxo group; namely, the pK_a value of the μ-OH of the $Os^{II}(\mu\text{-}OH)Os^{III}$ state is higher than 10.5, and that of the $Os^{III}(\mu\text{-}OH)Os^{III}$ state is lower than 5, and (ii) the redox potential of the $Os^{III}(\mu\text{-}O)Os^{III}/Os^{II}(\mu\text{-}O)Os^{III}$ process is more negative than that of $Os^{II}(\mu\text{-}OH)Os^{III}/Os^{II}(\mu\text{-}OH)Os^{II}$. Under such conditions, the bridging oxo group is protonated as soon as the one-electron reduction occurs at the potential for $Os^{III}(\mu\text{-}O)Os^{III}/Os^{II}(\mu\text{-}O)Os^{III}$ couple, and the

dx.doi.org/10.1021/ic201230k |*Inorg. Chem.* 2011, 50, 9014–9023

Scheme 2. Electrochemical Properties of μ-Oxo-μ-butyrato-diosmium Complex[a]

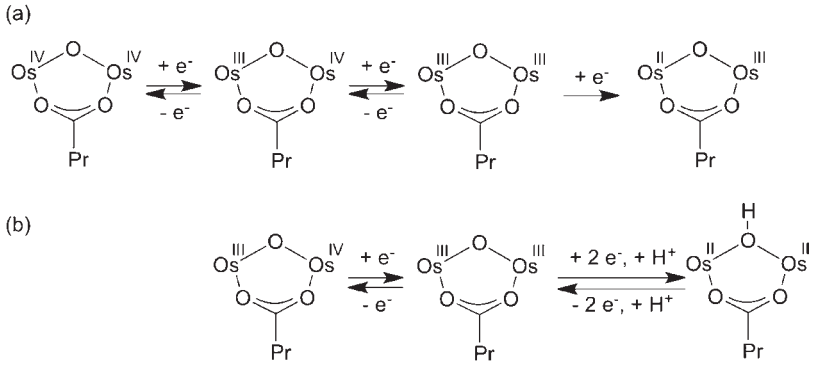

[a] (a) in CH_3CN and (b) in a H_2O-CH_3CN (1:1) mixed solvent.

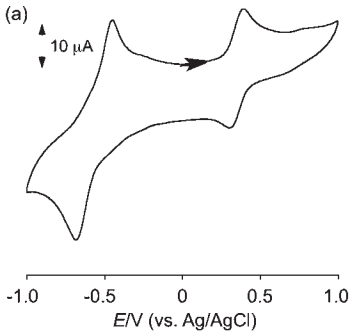

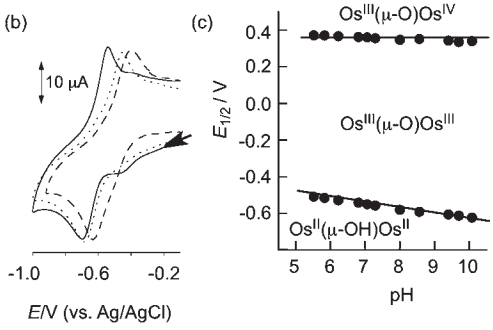

Figure 8. (a) Cyclic voltammogram of **1** in an acetonitrile/Britton−Robinson buffer (1:1) solution (pH 8.0) with a scan rate of 50 mV/s. (b) pH-Dependent redox wave change for the $Os^{III}Os^{III}/Os^{II}Os^{II}$ process; solid line: pH 10.1; dotted line: pH 8.0; dashed line: pH 5.5. (c) Potential−pH diagram for the $Os^{IV}Os^{III}/Os^{III}Os^{III}$ and $Os^{III}Os^{III}/Os^{II}Os^{III}$ processes in a pH range from 5.0 to 10.5.

resulting $Os^{II}(\mu\text{-OH})Os^{III}$ species is immediately reduced to $Os^{II}(\mu\text{-OH})Os^{II}$ at this potential. Although the pH dependence of the redox potential was not reported for the isostructural diruthenium analogue, such situations have been in fact reported in a μ-oxo-di-μ-acetato-diruthenium(III) complex, $[Ru^{III}_2(\mu\text{-O})(\mu\text{-CH}_3COO)_2(2,2'\text{-bipyridyl})_2(\text{pyridine})_2]^{2+}$, where proton-coupled electron transfer of $\{1H^+/2e^-\}$ occurs to give the corresponding μ-hydroxo-di-μ-acetato-diruthenium(II) species in an acidic solution.[20] On the other hand, the gold-surface self-assembled di-iron(III) analogue with the $[Fe^{III}_2(\mu\text{-O})(\mu\text{-RCOO})(tpa)_2]^{3+}$ fragment undergoes reduction involving a change of $\{1H^+/1e^-\}$ content to give $[Fe^{II}Fe^{III}(\mu\text{-OH})(\mu\text{-RCOO})(tpa)_2]^{3+}$ complex in the pH range 3−10.[21] Thus, it

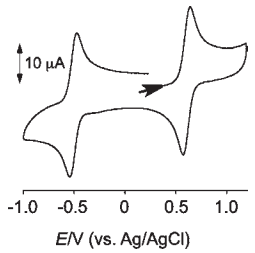

Figure 9. Cyclic voltammogram of **5** in acetonitrile containing $^nBu_4NPF_6$ (0.1 M) with a scan rate of 100 mV/s.

is suggested that the $Os^{II}(\mu\text{-OH})Os^{III}$ complex is less stable against disproportionation to the $Os^{II}(\mu\text{-OH})Os^{II}$ and $Os^{III}(\mu\text{-O})Os^{III}$ complexes ($K_{com} = [Os^{II}(\mu\text{-OH})Os^{III}]^2/[Os^{II}(\mu\text{-OH})Os^{II}][Os^{III}(\mu\text{-O})Os^{III}][H^+]$) as compared with the $Fe^{II}(\mu\text{-OH})Fe^{III}$ complex.

Complex ***5***. The di-μ-oxo-diosmium complex **5** showed two reversible redox waves in acetonitrile at $E_{1/2} = -0.53$ and +0.62 V vs Ag/AgCl as shown in Figure 9 (Table 5). The waves correspond to the redox couples of $Os^{III}Os^{III}/Os^{III}Os^{IV}$ and $Os^{III}Os^{IV}/Os^{IV}Os^{IV}$, respectively. The potentials are far more negative than those of the μ-oxo-μ-carboxylato-diosmiun complexes by about 1 V, indicating that the replacement of the second bridging ligand from carboxylate to the more basic oxide considerably stabilizes higher oxidation states. Although the redox potentials of **5** cannot be compared with those of the diruthenium analogue that is not known, the data are compared with those of the isostructural dirhenium complex. The corresponding redox potentials for the $[Re^{III}Re^{IV}(\mu\text{-O})_2(tpa)_2]^{3+}$ complex have been reported to be −0.77 V for $Re^{III}Re^{IV}/Re^{III}Re^{III}$ and +0.09 V for $Re^{III}Re^{IV}/Re^{IV}Re^{IV}$ vs Ag/AgCl, respectively,[11] in acetonitrile, indicating that the lower oxidation states are more stabilized in the diosmium complex. The difference of the redox potentials of the $M^{III}M^{IV}/M^{IV}M^{IV}$ processes is 0.53 V (= 0.62 (Os) − 0.09 (Re)) in the diosmium and dirhenium complexes, which is close to those of the M^{IV}/M^{III} or M^{III}/M^{II} processes in the mononuclear complexes, $[MCl_2(tpa)]^+$ (M = Os, Re).[15] However, that of the $M^{III}M^{IV}/M^{III}M^{III}$ processes between the two complexes is smaller (0.24 V = −0.53 (Os) − (−0.77, Re)) than that of the $M^{III}M^{IV}/M^{IV}M^{IV}$ processes. The difference between the two potentials of $Os^{III}Os^{IV}/Os^{III}Os^{III}$ and $Os^{III}Os^{IV}/Os^{IV}Os^{IV}$ of **5** is 1.15 V, from which the comproportionation constant (K_{com}) as

dx.doi.org/10.1021/ic201230k |*Inorg. Chem.* 2011, 50, 9014–9023

defined by eq 1 was calculated to be 5.9×10^{19}. The value is bigger by more than 6 orders of magnitude than the isostructural dirhenium analogue, $K_{com} = 1.5 \times 10^{13}$, indicating that the $Os^{III}Os^{IV}$ mixed-valent state is significantly more stable than the $Re^{III}Re^{IV}$ state of the dirhenium complex.[11] The different thermal stability of the mixed-valent states between the two complexes is ascribed to the nature of antibonding orbitals of the metal−metal bonds where the unpaired electron is located. Whereas the unpaired electron is localized in the δ^* orbital ($\sigma^2\pi^2\delta^2\delta^{*1}$) for the dirhenium complex, it is in the π^* orbital ($\sigma^2\pi^2\delta^2\delta^{*2}\pi^{*1}$) for the diosmium one. The unpaired electron may be stabilized by the π-orbital extended over the whole $Os_2(\mu\text{-}O)_2$ π-system. The K_{com} value of the di(μ-oxo)diosmium complex is close to those ($(1.8-3.9) \times 10^{19}$) of the μ-oxo-μ−carboxylato diosmium complexes (vide supra), suggesting that the corresponding osmium(III)osmium(IV) states have an unpaired electron in the π^* orbital. It is concluded that the larger stability of the osmium(III)osmium(IV) mixed-valent states is due to interactions of the π-type orbital occupied by an unpaired electron. It is also noted that the dinuclear osmium(III)osmium(IV) complex with a linear Os−O−Os unit (orbitals of π_1 and π_2 and π_1^* and π_2^* are almost degenerated in this case, and the unpaired electron is also located in one of the π^* orbitals) also gives a large K_{com} value (8.87×10^{19}),[7c] supporting these conclusions.

CONCLUSIONS

The present paper reported synthesis and characterization of oxo-bridged diosmium complexes of nitrogen-based tetradentate ligand (tpa). They cover μ-oxo-μ-carboxylate-diosmium(III) complexes, $[Os^{III}_2(\mu\text{-}O)(\mu\text{-}RCOO)(tpa)_2]^{3+}$ (R = C_3H_7, CH_3, and C_6H_5) and -osmium(III)osmium(IV) complex, $[Os^{III}Os^{IV}(\mu\text{-}O)(\mu\text{-}C_3H_7COO)(tpa)_2]^{4+}$ as well as di-μ-oxo-osmium(III)osmium(IV) complex, $[Os^{III}Os^{IV}_2(\mu\text{-}O)_2(tpa)_2]^{3+}$. The complexes with bridging carboxylates are the first examples of the μ-oxo-μ-carboxylato-diosmium complexes. The doubly oxo-bridged complex is also the first example of a mixed-valent di-μ-oxo-diosmium complex. The series of μ-oxo-μ-carboxylato-dimetal complexes has now been completed for group 8 elements Fe, Ru, and Os. The complex of $[Os^{III}Os^{IV}(\mu\text{-}O)(\mu\text{-}C_3H_7COO)(tpa)_2]^{4+}$ is a new member of oxidation number in the series. Within the series, the diruthenium and diosmium complexes exhibit a low spin state. X-ray structural study revealed increasing dπ−pπ interaction in the diosmium complex as evident from the increase in the M−O−M angle. From the redox potentials, higher oxidation states are increasingly stabilized in the diosmium complex. The pH-dependent cyclic voltammogram of the butylate complex indicated that the proton-coupled two-electron transfer is involved in the reduction of $[Os^{III}_2(\mu\text{-}O)(\mu\text{-}C_3H_7COO)(tpa)_2]^{3+}$ to yield a hydroxo-bridged diosmium(II) compound, $[Os^{II}_2(\mu\text{-}OH)(\mu\text{-}C_3H_7COO)(tpa)_2]^{2+}$. The significantly shorter osmium(III)−osmium(IV) bond distance than the sum of radii of two osmium atoms indicates the presence of a direct Os−Os bond. The bond order of 1.5 is suggested for the direct Os−Os bond of the di-μ-oxo complex by comparing the metal−metal distance with the isostructural rhenium(III)rhenium(IV) and dirhenium(IV) complexes.

ASSOCIATED CONTENT

Supporting Information. UV−vis spectra of **2** and **3** (Figures S1 and S2), cyclic voltammograms of **2** and **3** (Figures S3 and S4), and crystal data. This material is available free of charge via the Internet at http://pubs.acs.org.

AUTHOR INFORMATION

Corresponding Authors

*E-mail: sugimoto@mls.eng.osaka-u.ac.jp (H.S.), ysasaki@sci.hokudai.ac.jp (Y.S.), shinobu@mls.eng.osaka-u.ac.jp (S.I.).

ACKNOWLEDGMENT

This work was partly supported by a grant (Grant 22108520 to H.S.) for Scientific Research on Priority Areas "Coordination Programming" from MEXT of Japan and a grant (No. 23350027 to H.S.) for Scientific Research (B) from the Japan Society for Promotion of Science.

REFERENCES

(1) (a) Khan, M. I.; Zubieta, J. *Prog. Inorg. Chem.* **1995**, *43*, 1–150. (b) Perry, J. J.; Perman, J. A.; Zaworotko, M. J. *Chem. Soc. Rev.* 2009, *38*, 1400–1417. (c) Schubert, U. *Chem. Soc. Rev.* **2011**, *40*, 575–582.

(2) (a) Breedlove, B. K.; Yamaguchi, T.; Ito, T.; Londergan, C. H.; Kubiak, C. P. In *Comprehensive Coordination Chemistry II*; McCleverty, J. A., Meyer, T. J., Eds.; Elsevier: Amsterdam, Netherlands, 2004; Vol. 2, p 717. (b) Cao, R.; Han, J. W.; Andersson, T. M.; Hillesheim, D. A.; Hardcastle, K. I.; Slonkina, E.; Hedman, B.; Hodgson, K. O.; Kirk, M. L.; Musaev, D. G.; Morokuma, K.; Geletili, Y. V.; Hill, C. L. *Adv. Inorg. Chem.* **2008**, *60*, 245–272.

(3) (a) Gatteschi, D.; Caneschi, A.; Sessoli, R.; Cornia, A. *Chem. Soc. Rev.* **1996**, *25*, 101–109. (b) Neumann, R. *Prog. Inorg. Chem.* **1998**, *47*, 317–370.

(4) Gunay, A.; Theopold, K. H. *Chem. Rev.* **2010**, *110*, 1060–1081.

(5) Wu, A. J. J.; Penner-Hahn, E.; Pecoraro, V. L. *Chem. Rev.* **2004**, *104*, 903–938.

(6) Tshuva, E. Y.; Lippard, S. J. *Chem. Rev.* **2004**, *104*, 987–1012.

(7) (a) Chakravarty, A. R.; Cotton, F. A.; Schwotzer, W. *Inorg. Chem.* **1984**, *23*, 99–103. (b) Gilbert, J. A.; Geselowitz, D.; Meyer, T. J. *J. Am. Chem. Soc.* **1986**, *108*, 1493–1501. (c) Imbe, Y.; Umakoshi, K.; Matsunami, C.; Sasaki, Y. *Inorg. Chem.* **1995**, *34*, 813–820.

(8) Cotton, F. A.; Wilkinson, G.; Murillo, C. A.; Bochmann, M. *Advanced Inorganic Chemistry*, 6th ed.; John Wiley & Sons: New York, 1999; pp 1010−1039.

(9) Armstrong, J. E.; Robinson, W. R.; Walton, R. A. *Inorg. Chem.* **1983**, *22*, 1301–1306.

(10) Koshi, C.; Umakoshi, K.; Sasaki, Y. *Chem. Lett.* **1997** 1155–1156.

(11) Sugimoto, H.; Kamei, M.; Umakoshi, K.; Sasaki, Y.; Suzuki, M. *Inorg. Chem.* **1996**, *35*, 7082–7084.

(12) Takahira, T.; Umakoshi, K.; Sasaki, Y. *Acta Crystallogr., Sect. C: Cryst. Struct. Commun.* **1994**, *C50*, 1870–1872.

(13) Sugimoto, H.; Takahira, T.; Yoshimura, T.; Shiro, M.; Yamasaki, M.; Miyake, H.; Umakoshi, K.; Sasaki, Y. *Inorg. Chim. Acta* **2002**, *337* 203–211.

(14) (a) Norman, R. E.; Yan, S.; Que, L., Jr.; Backes, G.; Ling, J.; Sanders-Loehr, J.; Zhang, J. H.; O'Connor, C. J. *J. Am. Chem. Soc.* **1990**, *112*, 1554–1562. (b) Hazel, A.; Jensen, K. B.; McKenzie, C. J.; Toftlund, H. *Inorg. Chem.* **1994**, *33*, 3127–3134. (c) Wilkinson, E. C.; Dong, Y.; Que, L., Jr. *J. Am. Chem. Soc.* **1994**, *116*, 8394–8395.

(15) Sugimoto, H.; Matsunami, C.; Koshi, C.; Yamazaki, M.; Umakoshi, K.; Sasaki, Y. *Bull. Chem. Soc. Jpn.* **2001**, *74*, 2091–2099.

(16) SIR2008: Burla, M. C.; Caliandro, R.; Camalli, M.; Carrozzini, B.; Cascarano, G. L.; Caro, L. D.; Giacovazzo, C.; Polidori, G.; Siliqi, D.; Spagna, R. *J. Appl. Crystallogr.* **2007**, *40*, 609−613.

(17) *Crystal Structure 3.8: Crystal Structure Analysis Package*; Rigaku Corporation: The Woodlands, TX, 2000−2006.

(18) (a) Sasaki, Y.; Suzuki, M.; Tokiwa, A.; Ebihara, M.; Yamaguchi, T.; Kabuto, C.; Ito, T. *J. Am. Chem. Soc.* **1988**, *110*, 6251–6252. (b) Neubold, P.; Wieghardt, K.; Nuber, B.; Weiss, J. *Inorg. Chem.* **1989**, *28*, 459–467.

(19) Wells, A. F. *Structural Inorganic Chemistry*, 5th ed.; Clarendon Press: Oxford, U. K., 1984.

(20) Uehara, H.; Abe, M.; Hisaeda, Y.; Uosaki, K.; Sasaki, Y. *Chem. Lett.* **2006**, *35*, 1178–1179.

(21) Inomata, T.; Abe, M.; Kondo, T.; Umakoshi, K.; Uosaki, K.; Sasaki, Y. *Chem. Lett.* **1999**, 1097–1098.